Article

Engineered Protein-Driven Synthesis of Tunable Iron Oxide Nanoparticles as T1 and T2 Magnetic Resonance Imaging Contrast Agents

Antonio Aires,* Yilian Fernández-Afonso, Gabriela Guedes, Eduardo Guisasola, Lucía Gutiérrez, and Aitziber L. Cortajarena*

Read Online

ACCESS | Metrics & More | Article Recommendations | Supporting Information

ABSTRACT: Iron oxide nanoparticles (IONPs) have become one of the most promising nanomaterials for biomedical applications because of their biocompatibility and physicochemical properties. This study demonstrates the use of protein engineering as a novel approach to design scaffolds for the tunable synthesis of ultrasmall IONPs. Rationally designed proteins, containing different number of metal-coordination sites, were evaluated to control the size and the physicochemical and magnetic properties of a set of protein-stabilized IONPs (Prot-IONPs). Prot-IONPs, synthesized through an optimized coprecipitation approach, presented good T1 and T2 relaxivity values, stability, and biocompatibility, showing potential for magnetic resonance imaging (MRI) applications.
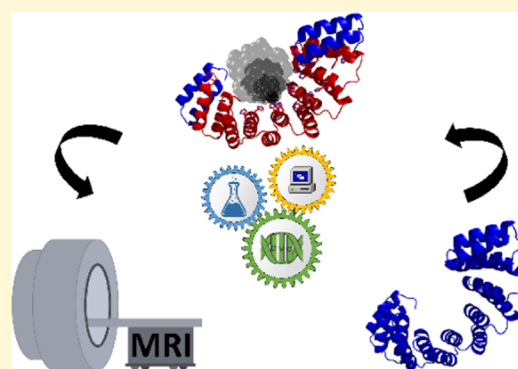
INTRODUCTION

In the last century, many different nanomaterials have been widely investigated. Among the different types of nanomaterials, magnetic nanoparticles (MNPs) have aroused great interest because of their widespread scientific applications (data and energy storage,[1,2] catalysis,[2,3] environmental remediation,[4,5] magnetic fluids,[6,7] electronics,[8,9] and biomedicine[10,11]). Especially, iron oxide nanoparticles (IONPs) have been extensively pursued in biomedicine owing to their physicochemical properties, stability, and biocompatibility.[12–14] In this context, IONPs have been frequently used in different biomedical applications such as MRI,[15,16] magnetic particle imaging (MPI),[17,18] bioseparation,[19,20] biosensing,[21,22] and therapy (hyperthermia,[23,24] drug,[25,26] and gene delivery[27,28]).

The particle size, shape, and purity of IONPs are critical parameters for their successful application in biomedicine because these factors strongly affect their physicochemical properties and their biocompatibility. Therefore, the development of reliable and reproducible methods to synthesize uniform-sized IONPs has been one of the major challenges in this field over the last few years. Methods to achieve monodisperse and size-controlled IONPs usually need extreme reaction conditions and harsh chemicals.[12,29–33] This means that the inorganic synthesis of IONPs is often not easy to scale-up, costly, environmentally harmful, and needs post-synthetic steps. Alternative IONP synthesis procedures using mild conditions are difficult to control, whereas coprecipitation

methods produce IONPs with a broad range of shapes and sizes. Therefore, despite the great efforts made toward the development of straightforward and reproducible synthetic procedures, the resulting IONPs are usually unsuitable for biomedical applications.[12]

The necessity to improve the uniformity and biocompatibility of IONPs has recently focused research interest on biologically controlled mineralization as a sustainable alternative to inorganic synthesis. A broad range of organisms is able to precisely drive the synthesis of different minerals under mild conditions.[34–36] In detail, the formation of biominerals and their structures are controlled by different biomolecules (polysaccharides, lipids, and proteins).[34] Those biomineralizing biomolecules have been employed as scaffolds to synthesize inorganic materials in vitro.[37] In the case of IONPs, the magnetotactic bacterium *Magnetospirillum magneticum* forms highly uniform IONPs through biomineralization proteins located within the magnetosome membrane.[38–42] One of these proteins, Mms6, contains a natural metal-binding site, which binds iron ions, nucleating and controlling the *in vivo* formation of magnetite.[42,43] It has also been demonstrated
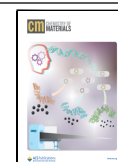
that purified Mms6 controls the formation of magnetite IONPs in vitro through a coprecipitation procedure at room temperature.[42−46] However, to date, the templating of IONPs using biomolecules has been limited to naturally occurring (e.g., magnetosome proteins) or commercially available peptides and proteins (e.g., bovine serum albumin), leaving the field of designed proteins largely unexploited. The utilization of designed proteins to template IONPs holds a huge potential since, in addition to all of the known advantages of the use of biomolecules, it can also provide control over the coordination and synthesis of IONPs, allowing fine-tuning of their final properties, and ultimately tailoring of their specific applications.

Herein, we describe a novel approach to template the synthesis of IONPs using engineered proteins. For this purpose, consensus tetratricopeptide repeat (CTPR) proteins were employed as the basic protein unit that was further engineered to display metal-coordination sites. In particular, here, we report the engineering of an iron-binding protein (Figure 1A), which was designed based on peptides rich in acidic residues from natural coordination systems. The

templating of IONPs was comparatively studied using three other CTPR proteins (Figure 1B) previously described by our group.[47−51] The purpose of this study was not only to develop a reproducible and straightforward method for the production of IONPs stabilized by designed proteins (Prot-IONP) but also to evaluate the influence of the nature and size of the metal-coordination sites in the physicochemical properties of the resulting Prot-IONP complexes (e.g, oxidation state and relaxivity). Moreover, thanks to the modular properties of the CTPR module, the tunability of the size of the resulting IONPs was also evaluated using proteins with different sizes. Finally, as a proof of concept of the applicability of the developed Prot-IONPs as MRI contrast agents, the relaxivity parameters of different systems were evaluated.

This paper constitutes pioneering work in the field of IONPs since it describes how their properties can be tailored according to the chemical environment and size of the templating biomolecules, ultimately leading to the development of improved nanomaterial hybrids for biomedical applications.

■ RESULTS AND DISCUSSION

In this study, the design and incorporation of an iron-coordination site in the CTPR scaffold protein were investigated as templates to synthesize Prot-IONPs. The iron-coordination site was based on the natural iron-binding site present in the Mms6 protein,[53] and comprised four coordinating glutamic acids. This site was modeled and incorporated within the CTPR protein structure (PDB ID: 1Na0).[54] First, as the CTPR sequence already contains several residues that can bind iron ions (lysines (K), aspartic (D), and glutamic acids (E)), a minimalist CTPR module (Cmin) was generated by keeping the conserved amino acids that encode the protein fold[54,55] and replacing most of the others by alanine (Supporting Information). Then, four glutamic acids were introduced, at specific positions within the minimalist CTPR module (2, 5, 6, and 9) to keep encoding a metal-coordination site like the one observed in the Mms6 protein,[53,56] generating the Cmin_4E module (E_4) (Figure 1A). Finally, the engineered E_4 module was assembled into a CTPR protein composed of six iron-binding E_4 modules framed by two non-modified CTPR modules (W), as capping modules, generating the CTPR8-W(E_4)$_6$W (C8-24E) protein (Figure 1A). The C8-24E protein was expressed in *Escherichia coli* C41 (DE3) obtaining good yields (50 mg/L) of a soluble and properly folded protein (see the CD spectrum in the Supporting Information). The C8-24E protein was evaluated as a scaffold for the synthesis of IONPs. To unravel the influence of the metal-coordinating residues on the magnetic and physicochemical properties of the resulting Prot-IONP, the resulting nanomaterials were compared with the ones obtained using previously designed metal-binding proteins based on histidines (C8-24His) or cysteines (C8-24Cys), and a wild-type CTPR protein containing several residues that can bind iron ions (lysines and aspartic and glutamic acids) (C8-Wt) (Figures 1B and S1).[47−51]

An optimized coprecipitation protocol based on a previously reported procedure was evaluated for the synthesis of biocompatible Prot-IONPs (Figure 1C, procedure in the Supporting Information).[52] This procedure consists of two main steps: in the first step, the iron salts are mixed with the metal-binding proteins. This mixture is incubated to allow coordination of iron to the metal-binding residues. In a second
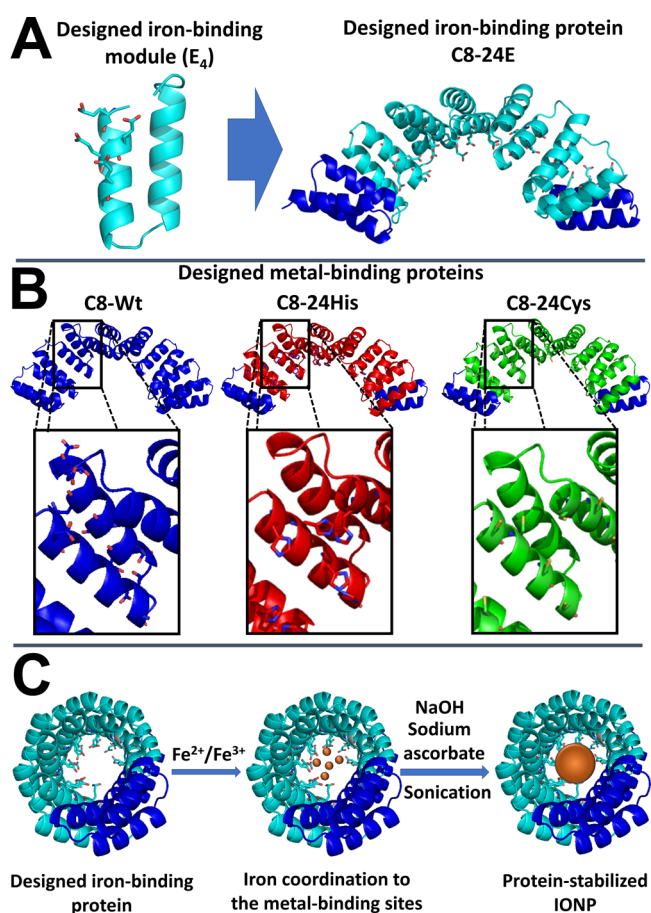
Figure 1. Designed CTPR proteins used to synthesize Prot-IONP. (A) Modified minimalistic CTPR module in which glutamic acids were introduced at positions 2, 5, 6, and 9 (E_4 module). CTPR8 protein composed of E_4 (cyan) and Wt (blue) modules. (B) Previously designed metal-binding proteins based on histidine (C8-24His), cysteines (C8-24Cys), and the wild-type CTPR protein containing several residues that can bind iron ions (C8-Wt). (C) General scheme for the synthesis of IONPs by an optimized coprecipitation method.[52]
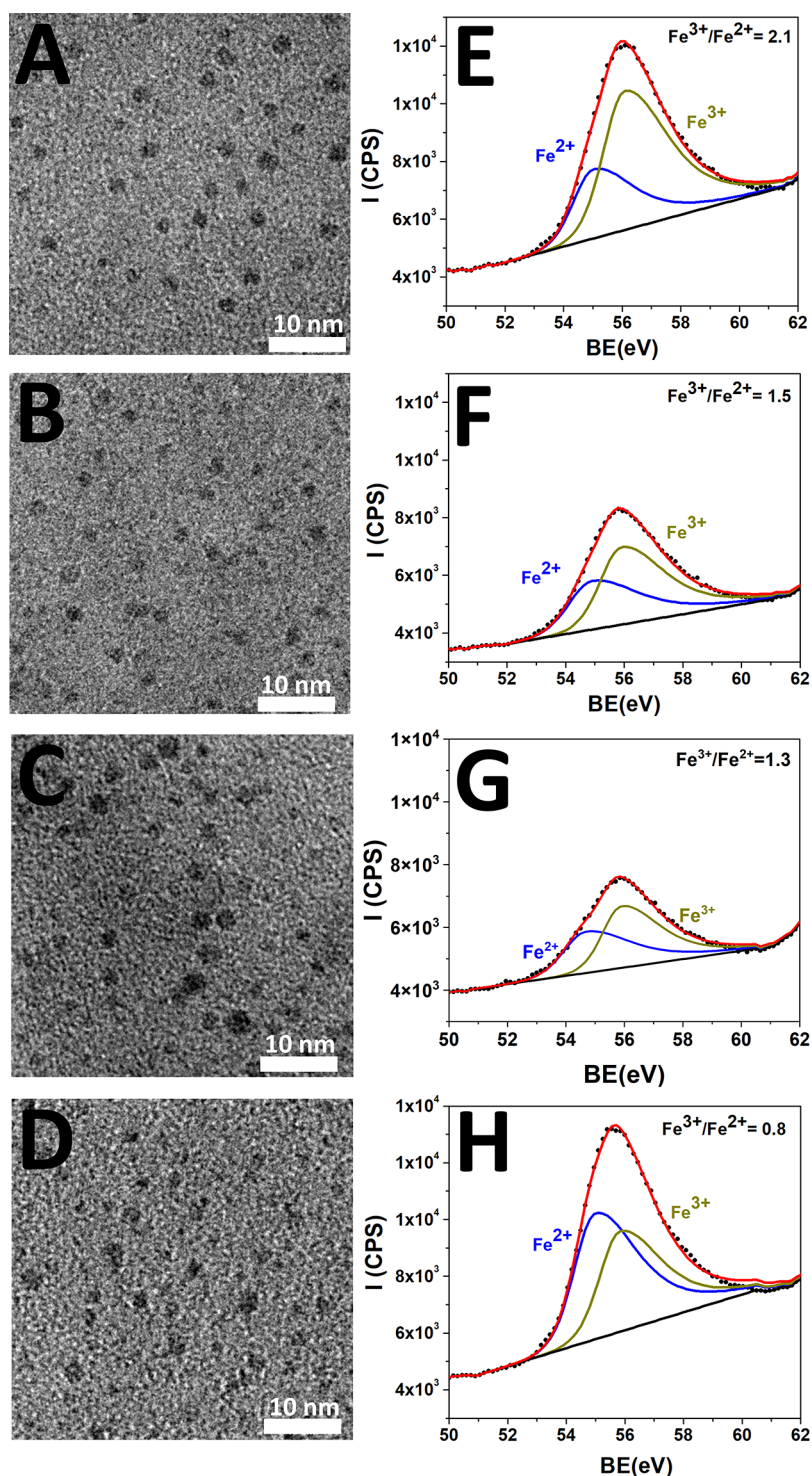
Figure 2. TEM images and XPS spectra of the Prot-IONPs synthesized using the C8-24E (A, E), C8-Wt (B, F), C8-24His (C, G), and C8-24Cys (D, H) proteins. TEM scale bars: 10 nm. The XPS spectra of the Prot-IONPs show the Fe 3p peaks (red line) and their deconvolution into Fe(III) (green line) and Fe(II) (blue line) components.

step, sodium hydroxide and sodium ascorbate are introduced in the reaction that is subsequently sonicated at 65 °C to promote the coprecipitation and formation of highly crystalline IONPs.

The formation of Prot-IONPs was verified using transmission electron microscopy (TEM) (Figures 2A−D and S2). As shown in Figure 2, Prot-IONPs presented a spherical shape with a core size of 2.2 ± 0.3 (C8-24E), 2.0 ± 0.2 (C8-Wt), 2.4

± 0.3 (C8-24-His), and 2.1 ± 0.3 nm (C8-24Cys), respectively (Figure 2A−D), suggesting that the nature of the metal-binding sites did not influence the core size of the resulting Prot-IONPs. The synthesis in the absence of proteins showed the formation of unstable IONPs that tend to form large aggregates (Figure S3).

The integrity of the protein scaffold after the synthesis of Prot-IONPs, which is the key for biomedical applications,[57,58]

was verified by circular dichroism (CD). The CD spectra of the protein scaffolds presented the characteristic signature of well folded α-helical structures (Figure S4). The CD spectra of the Prot-IONPs were very similar to the CD spectra of the original proteins, indicating that the IONP synthesis did not affect their α-helical structure (Figure S4).

To study the efficiency of Prot-IONPs as MRI contrast agents, relaxivity measurements were performed under 1.5 T at room temperature (Table 1 and Figure S5). The transversal

Table 1. Relaxometric Values for the Prot-IONP

| Prot-IONP	r_1 (mM^{-1} s^{-1})	r_2 (mM^{-1} s^{-1})	r_2/r_1	size (nm)
C8-24E-IONP	1.98	2.32	1.17	2.2 ± 0.3
C8-Wt-IONP	2.24	2.66	1.19	2.0 ± 0.2
C8-24His-IONP	3.50	4.10	1.17	2.4 ± 0.3
C8-24Cys-IONP	3.04	3.45	1.13	2.1 ± 0.3

and longitudinal relaxivities (r_2 and r_1, Table 1) show that Prot-IONPs presented moderate r_2 and r_1 values, while their r_2/r_1 ratios were low. These moderate longitudinal relaxivity and low r_2/r_1 ratios suggest their potential as T_1 contrast agents. The Prot-IONPs stabilized by C8-24His protein showed the best relaxivity values, having similar properties to some of the clinically approved T_1 contrast agents and novel IONPs described in the current state of the art.[59−61] For example, MultiHance, an approved Gd-based T_1 contrast agent has r_2 and r_1 values of 4.3 and 4.0 mM^{-1} s^{-1}, respectively (1.5 T).[59]

To understand the phenomenon behind the change in the relaxivity values of the Prot-IONP, X-ray photoelectron spectroscopy (XPS) measurements were performed to determine if the composition of the inorganic core influenced their efficiency as T1 contrast agents. The XPS spectra of Prot-IONPs (Figure 2E−H) showed a band at a binding energy (BE) of around 55.5 eV (Fe 3p). The quantitative deconvolution of the Fe 3p peaks into Fe(III) and Fe(II) components presented two BEs of 55.0 and 56.0 eV (Figure 2E−H), indicating that the IONPs presented a mixture of Fe(III) and Fe(II) in a Fe(III)/Fe(II) ratio of 2.1 (C8-24E), 1.5 (C8-Wt), 1.3 (C8-24His), and 0.8 (C8-24Cys), respectively (Figure 2E−H).

These results indicate that the nature of the metal-binding site influences the composition of the Prot-IONP. As the reducing power of metal-coordination residues increased (E<H<C), the Fe(III)/Fe(II) ratio decreased.[62] Here, the WT protein is not being considered since there are several amino acids involved in the iron coordination and it is difficult to discriminate the role of each of them. In addition, the Fe 2p XPS spectra of Prot-IONPs (Figure S6) showed the expected position of the Fe-O bonds, at around 710.8 eV and Fe-Fe around 707 eV with no satellite peaks (Figure S6).[63] The Fe 2p peak of Fe_3O_4-like materials do not show significant satellite peaks, while Fe_2O_3-like materials show satellite and shake-peaks at 719 and 733 eV,[64] suggesting that their iron cores were mainly composed of magnetite (Fe_3O_4).

To further explore the different relaxometry behaviors observed, the magnetic properties of the Prot-IONPs were analyzed, as such properties are strongly affected by the particle size, crystallinity, and composition, and this fact is correlated with their relaxivity performance.[65] Field-dependent magnetization cycles at 300 K together with temperature-dependent AC magnetic susceptibility measurements were performed

(Figures 3 and S7). All of the Prot-IONPs were super-paramagnetic at 300 K and showed very low saturation
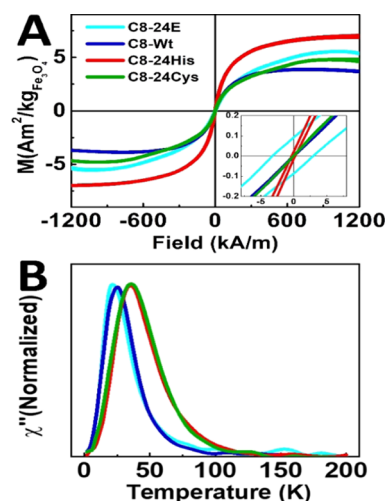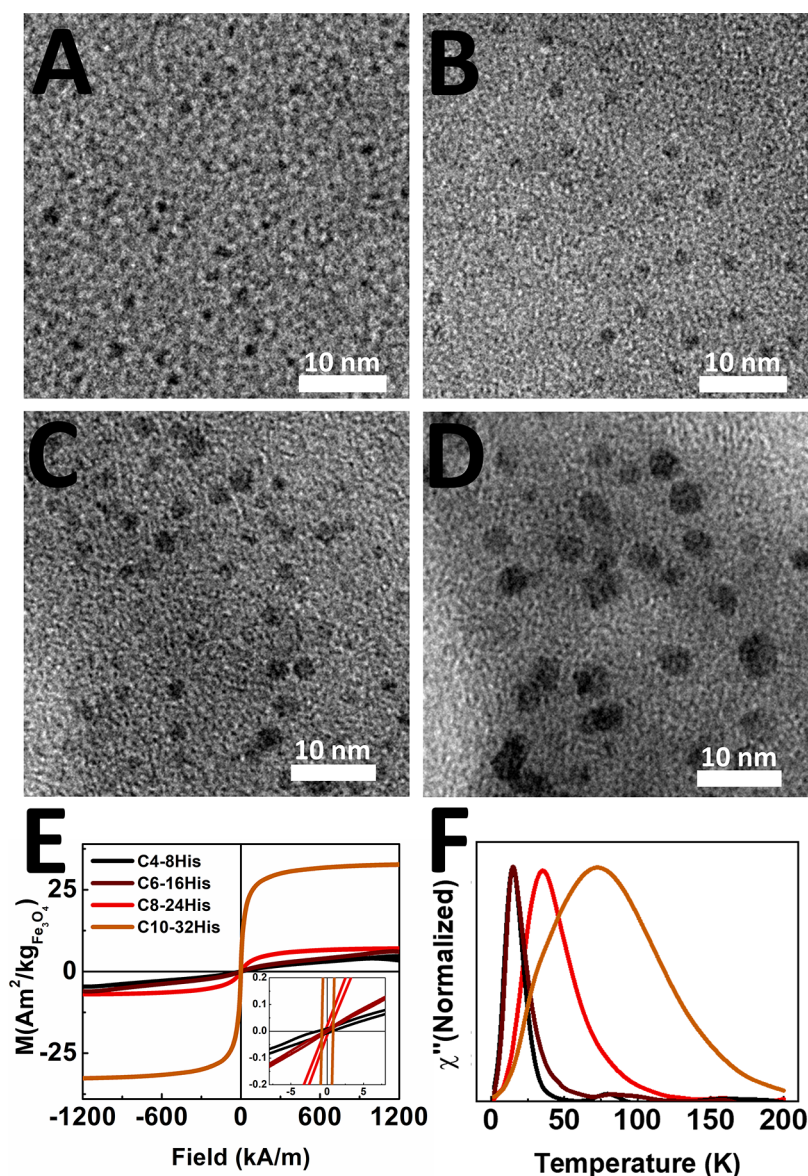

Figure 3. (A) Field-dependent magnetization and (B) temperature dependence of the normalized out-of-phase magnetic susceptibility of the Prot-IONPs synthesized using C8-24E (cyan), C8-Wt (blue), C8-24Cys (green), and C8- 24His (red) proteins.

magnetization (M_s) values, in agreement with their small size.[66] The highest M_s value corresponded to C8-24His (Figure 3A), with a M_s of 7 Am^2/kg$_{Fe3O4}$, over 10 times lower than bulk magnetite. C8-24His was also the Prot-IONP with the highest blocking temperature in the AC magnetic susceptibility measurements (Figure 3B), in agreement with their higher r_2 values, as relaxivity and the blocking temperature depend on the same parameters.

Finally, as the metal-binding protein that produced IONPs having the best relaxivity values was C8-24His, the effect of the size of the protein scaffold on the physicochemical and magnetic properties of the Prot-IONPs was studied. For this purpose, an array of proteins containing 2, 4, 6, and 8 metal-coordination modules based on histidines (C4-8His, C6-16His, C8-24His, and C10-32His), was designed and evaluated (Figures 4A−D and S9). In particular, the metal-binding protein C10-32His, which is described for the first time in this work, was soluble, showed the expected MW as measured by MALDI-TOF, and was properly folded as indicated by its CD spectra (Figure S10). TEM images (Figures 4A−D and S11) show that the resulting Prot-IONPs presented metal-core sizes of 1.1 ± 0.3 (C4-8His), 1.7 ± 0.2 (C6-16His), 2.4 ± 0.3 (C8-24His), and 4.0 ± 0.4 nm (C10-32His), respectively. This increase of the metal-core size (from 1 to 4 nm) of the Prot-IONP when the size of the protein scaffold and the number of the metal-coordination modules increased, suggesting that the metal-core size is modulated by the size of the designed protein scaffold (Figures 4A−D and S11). Additionally, C10-32His-IONPs were also analyzed by high-resolution TEM (HRTEM) to prove the crystalline structure of IONPs (Figure S12).

To evaluate the influence of the IONP size on the performance of Prot-IONPs as MRI contrast agents, relaxivity measurements were performed under 1.5 T in a nuclear magnetic resonance spectrometer at room temperature (Table 2 and Figure S13).

Table 2 shows that all of the protein-IONPs presented moderate r_1 (from 1 to 6 mM^{-1} s^{-1}) and moderate r_2 (from 1

Figure 4. (A−D) TEM images of Prot-IONPs synthesized using C4-8His (A), C6-16His (B), C8-24His (C), and C10-32His (D) proteins. Scale Bars 10 nm. (E). Field-dependent magnetization and (F) temperature dependence of the normalized out-of-phase magnetic susceptibility of Prot-IONPs synthesized using the C4-8His (black), C6-16His (brown), C8-24His (red), and C10-32His (orange) proteins.

Table 2. Relaxometric Properties of Prot-IONPs Synthesized Using C4-8His, C6-16His, C8-24His, and C10-32His Proteins

Prot-IONP	r_1 (mM^{-1} s^{-1})	r_2 (mM^{-1} s^{-1})	r_2/r_1	size (nm)
C4-8His-IONP	1.02	1.25	1.14	1.1 ± 0.3
C6-16His-IONP	2.11	2.54	1.22	1.7 ± 0.2
C8-24His-IONP	3.50	4.10	1.17	2.4 ± 0.3
C10-32His-IONP	6.13	61.60	10.05	4.0 ± 0.4

to 4 mM^{-1} s^{-1}) values except in the case of C10-32His-IONPs, which presented a high r_2 value (60 mM^{-1} s^{-1}). Moreover, an increase in the relaxivity values of Prot-IONPs was observed when their metal-core size increased, from 1 to 4 nm, as previously reported for other systems.[66] All of the Prot-IONPs presented low r_2/r_1 values (from 1.14 to 1.22) except for C10-32His-IONPs, which showed a high value (10.05).

The moderate longitudinal relaxivities and low r_2/r_1 values for C4-8His-IONPs, C6-16His-IONPs, and C8-24His-IONPs suggest their potential as T_1 contrast agents. Differently, the high transverse relaxivity and high r_2/r_1 value for C10-32His-

Prot-IONPs indicate their great potential as a T_2 contrast agent, since it displays high r_2 values that can be explained in view of their larger size (4 nm). These findings are in agreement with the IONP metal-core size limit previously described for T_1 or T_2 contrast agents, between 2.5 and 5 nm.[66,67] These relaxivity values are similar to some of approved IONP contrast agents used in clinics.[59−61] For example, Feridex, a clinically approved IONP-based contrast has r_2 and r_1 values of 41 and 4.7 mM^{-1} s^{-1}, respectively (1.5 T).[59]

Moreover, the different relaxivities observed for this series were in concordance with the Prot-IONP magnetic properties.

Field-dependent magnetization measurements at 300 K showed that C10-32His had a much larger M_s value (33 Am^2/kg_{Fe3O4}) than the rest of the Prot-IONPs, with M_s values between 4 and 7 Am^2/kg_{Fe3O4} (Figure 4E). This result highlights the necessity of keeping low M_s values for IONPs to produce T_1 contrast agents. A relationship between the particle size and both their susceptibility at low field strengths (inset Figure 4E) and their blocking temperature in the AC magnetic susceptibility data (Figures 4F and S8) was found. The small differences in the particle average size (less than 3 nm between the smallest and biggest Prot-IONPs of this series) resulted in clear differences in their magnetic properties. These results indicated that the frontier between T_1 and T_2 contrast agents based on IONPs is between 2.5 and 4 nm, in agreement with previous works evaluating IONPs in the same size range.[66]

CTPR proteins are repeat proteins constituted by 34 amino acid repeats that fold into a helix-turn-helix motif. Repeated CTPR modules form a superhelical structure with 8 repeat per superhelical turn, in which each repeat contributes to approximately 1 nm length (*i.e.* a 10-repeat protein C10 is approx. 10 nm long). Considering that the design includes for stability purposes two WT capping repeats at the terminal ends, within a C10 there are 8 metal-coordinating repeats, with 4 coordinating amino acids each within the concave face. This results in a coordination length of around 8 nm. The coordination of the metals occurs in the confined inner part of the superhelix providing larger surface protection to IONPs and tunability of the nanoparticle size. The results reported here confirm the correlation between the increase in protein size and the increase in the metal-core size of the resulting Prot-IONP.

Finally, the potential of Prot-IONPs (C8-24His-IONPs and C10-32His-IONPs) as contrast agents for *in vivo* applications was evaluated for studying their MRI performance, stability under physiological conditions, and biocompatibility. T_1- and T_2-weighted MRI images measured in PBS on a 7-T MRI scanner at room temperature showed a clear relationship between the signal intensity and the iron concentration (Figure 5A,B), confirming the efficiency of Prot-IONPs as T_1 or T_2 contrast agents.

Then, the stability of Prot-IONPs under *in vivo*-like conditions was tested by monitoring the T_2 relaxation over time (Figure 5C), as the T_2 relaxation time is very sensitive to the contrast agent stability (aggregation state of IONPs).[68,69] Moreover, the morphology and crystallinity of Prot-IONPs were also evaluated (Figure S12) to further prove the stability and absence of aggregation of the developed protein–nanomaterial hybrids at least for a week at 37 °C in the physiological medium and 6 months in water in the fridge. Figure 5C shows that Prot-IONPs presented excellent stability, since their T_2 relaxation times did not change during at least 5 days under physiological conditions. Finally, the cytotoxicity of the Prot-IONPs was tested on NIH-3T3 fibroblast cells, at different Prot-IONP concentrations (1-20 μM) under standard cell culture conditions (Figure 5D). Figure 5D shows that after 4 days of incubation, Prot-IONPs did not produce cytotoxicity or evident morphological changes in the NIH-3T3 fibroblasts.

■ CONCLUSIONS

In summary, this work explores the novel use of designed metal-binding CTPR proteins as scaffolds to produce ultra-small, uniform, stable, and biocompatible Prot-IONPs for
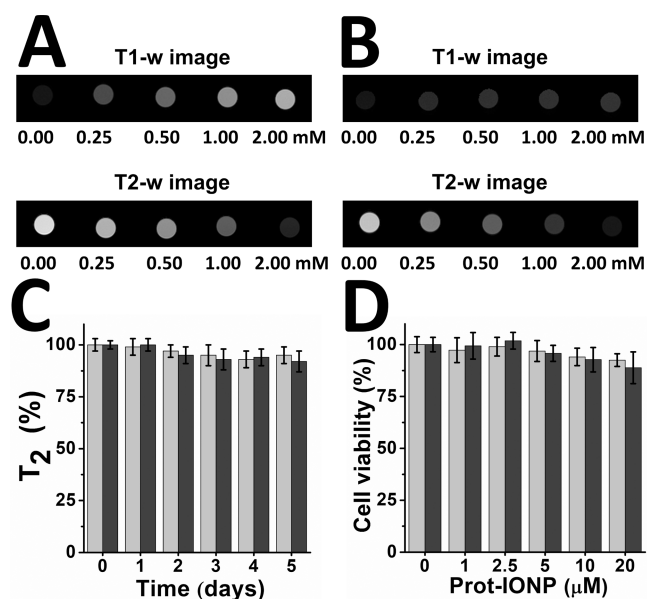
Figure 5. (A, B) T1- and T2-weighted images of the Prot-IONPs synthesized using C8-24His (A) and C10-32His (B) proteins, showing the dependence of the signal with the iron concentration. (C) Stability of the Prot-IONPs synthesized using the C8-24His (gray) and C10-32His (black) proteins expressed as the percentage of change of the transverse (T2) relaxation time over the time (T_2 measured at 1.0 mM of Fe). (D) Cytotoxicity of the Prot-IONPs synthesized using the C8-24His (gray) and C10-32His (black) proteins evaluated on NIH-3T3 fibroblast cells.

future biomedical applications. An array of rationally designed metal-binding proteins was evaluated demonstrating that (1) the metal-coordination residues can modulate the chemical composition of Prot-IONPs and, therefore. modified their physicochemical and magnetic properties and (2) the size of the protein scaffold determines the IONP metal-core size. The synthetic procedure explored here, allowed us to synthesize biocompatible Prot-IONPs stable under physiological conditions, showing their efficiency as T_2 and T_1 MRI contrast agents for biomedical applications. Overall, the novel strategy presented here to develop Prot-IONPs shows the potential of designed protein–nanomaterial hybrids, opening up novel and sustainable paths to control and tune the synthesis of novel nanomaterial for their application as MRI contrast agents.

■ GENERAL METHODS

Protein Design, Cloning, and Molecular Biology. The minimalistic CTPR module (Cmin) (AAAWAALAAAYA ASG-NYAAAIAAYAAALAANPRS) was created in two steps using Klenow extension and overlapping polymerase chain reaction (PCR).[70] First, two Klenow extensions were performed to generate two Klenow fragments, and second, the resulting Klenow fragments were assembled using overlapping PCR. The C1_min module, comprises one CTPR repeat with an N-terminal extension (GAMGS), and a C-terminal helix to improve its solubility (AAAAAALAAAAAAQA). C1_A2E_A5E_A6E_A9E (Cmin-4E) (AEAWEELAEA YAASG-NYAAAIAAYAAALAANPRS) was prepared from the previously described C1_min module by QuikChange Site-Directed muta-genesis. By a combination of the Cmin_4E (E4) modules and wild-type CTPR modules (Wt), CTPR8-W(E4)6W (C8-24E) was generated. For this purpose, DNA encoding the E4 and Wt modules was fused using *Bam*HI and *Bgl*II in the pProEx-HTA vector.[71] Finally, the gene sequence was verified by DNA sequencing (Stab

Vida). CTPR metal-binding protein scaffolds were generated as previously described.[47]

Protein Expression and Purification. Proteins were expressed and purified as previously described.[47]

SDS-PAGE Gel Electrophoresis. The samples were run on a 15% acrylamide gradient gel at 150 V and the gel was visualized under a UV transilluminator and after Coomassie blue staining.

Synthesis of Protein-Stabilized Iron Oxide Nanoparticles (Prot-IONPs). Prot-IONPs were synthesized through a coprecipitation approach based on a previously reported method.[52] Briefly, 1 mL of the protein scaffold at 45 μM was mixed with a 2:1 mixture of $FeCl_2 \cdot 4H_2O$ and $FeCl_3 \cdot 6H_2O$ (6 eq. respect to Glu metal-binding residues) under a nitrogen atmosphere. Then, the reaction mixture was incubated for 30 min at room temperature and a 0.1 mM NaOH solution was added until a pH value equal to 10 was reached. Then the reaction was sonicated for 10 min at 65 °C, and a solution of sodium ascorbate (10 equiv with respect to iron ions) was added to the reaction mixture, which was again sonicated for 10 min at 65 °C. Finally, Prot-IONPs were purified by gel filtration using a PD-10 column containing Sephadex G-25 resin (Cytiva).

Circular Dichroism (CD). The secondary structure of the designed proteins and Prot-IONPs was measured by CD as previously described.[47] The measurements were performed on a Jasco J-815 spectrometer (JASCO Corporation, Tokyo, Japan) at a protein concentration of 5 μM, in a cuvette with 1 mm path length, at 25 °C using a bandwidth of 1 nm with increments of 1 nm and 10 s average time.

Inductively Coupled Plasma Mass Spectrometry (ICP-MS). The Fe concentration of the Prot-IONPs was measured, after acid digestion of the samples. In brief, to 50 μL of each sample at a protein concentration of around 50 μM were added 300 μL of 37% HCl. This mixture was sonicated for 30 min at 40 °C, and afterward diluted to 3.1 mL with bi-distilled water. The ICP-MS measurements were taken using an iCAP-Q ICP-MS (Thermo Scientific, Bremen, Germany) equipped with an autosampler ASX-520 (Cetac Technologies Inc., NE) ($n = 3$) and QtegraTM v2.6 (Thermo Scientific).

Transmission Electron Microscopy (TEM). TEM samples were prepared and recorded as previously described.[47] The samples were imaged using ultrathin carbon films on copper grids (TED PELLA INC.), that were first treated with glow discharge. Then the sample was deposited by drop-casting 40 μL of sample solution. Micrographs were recorded using a JEOL JEM 2100F electron microscope operating at 200 kV with a Field Emission Gun.

X-ray Photoelectron Spectroscopy (XPS). XPS experiments were performed as previously described.[47] A SPECS Sage HR 100 spectrometer with a non-monochromatic X-ray source (aluminum Kα line of 1486.6 eV energy and 251 W) was used to acquire the spectra. The analysis was performed by placing the samples perpendicularly to the analyzer axis and calibrated using the $3d_{5/2}$ peak of Ag with a full width at half maximum (FWHM) of 1.1 eV. The spectra were acquired with a resolution of 15 eV of Pass Energy and 0.15 eV/step. The measurements were performed in an ultrahigh vacuum (UHV) chamber at a pressure lower than 8×10^{-8} mbar. The quantification of Fe^{3+} and Fe^{2+} species was performed according to Yamashita et al.[72] The spectra were initially treated with a linear background correction and then fitted using asymmetric functions, in which the FWHM of the peaks were limited while the peak positions and areas were unconstrained. For charge correction, the peak of the Carbon 1s was set to 284.8 eV.

MRI Measurements. Prot-IONPs were characterized in terms of their magnetic properties using a 1.5 T Time-Domain (TD) NMR benchtop system (Bruker Minispec mq20). The samples were analyzed by placing 300 μL of several Prot-IONP dilutions in 10 mm diameter NMR glass tubes. To determine T1 and T2 relaxation times, standard CPMG and saturation recovery sequences were used, respectively. R_1 and R_2 relaxation rates (R) were determined as 1000/T1 or T2 respectively, while r_1 and r_2 relaxivities (r) correspond to the angular coefficient of the calibration curve R vs concentration, obtained from 5 different solutions.

T1- and T2-Weighted MRI Images. The acquisition of T1- and T2-weighted MR images was performed by a 7-T Bruker Biospec 70/30 USR MRI system (Bruker Biospin GmbH, Ettlingen, Germany), interfaced to an AVANCE III console. The image acquisition employed a BGA12 imaging gradient (maximum gradient strength of 400 mT/m) and a 40 mm diameter quadrature volume resonator. The obtention of the T2 maps of the phantoms was done using Bruker's MSME (Multi slice Spin echo) sequence. The TE values ranged from 9 to 720 ms in 80 steps, and the TR was 10,000 ms.

The T1 maps of the phantoms were acquired using Spin echo saturation recovery using a variable repetition time Bruker's RAREVTR method. Images were acquired at 16 different TR values (10,000, 7000, 4500, 3000, 1800, 1200, 900, 700, 550, 450, 360, 300, 220, 150, 100, 51 ms), TE of 9 ms, and a RARE factor of 1.

All data were acquired with 2 averages, 360 × 360 points, and a Field of View of 3.6 cm × 3.6 cm, 3 slices were acquired with a slice thickness of 2.0 mm and a gap between slices of 2 mm.

T_1 and T_2 values were calculated by fitting the images into the Levenberg–Margardt method and then determined using Bruker's Paravision 6.0.1 software.

Magnetic Characterization. A known volume of each Prot-IONP was deposited into a piece of cotton wool and dried at room temperature. Then, the samples were placed inside gelatin capsules for their characterization. Magnetic measurements were performed using a MPMS-XL SQUID magnetometer (Quantum Design). Field-dependent magnetization was recorded in the field range between −1200 and 1200 kA/m at 300 K. The temperature dependence of the AC magnetic susceptibility was measured from 2 to 200 K, using a magnetic field amplitude of 4.1 Oe and a frequency of 11 Hz.

Stability of the Prot-IONPs under Physiological Conditions. The stability of the Prot-IONPs under physiological conditions was evaluated, during 5 days at 37 °C, by monitoring the transverse (T2) relaxation times using a 1.5 T Time-Domain (TD) NMR benchtop system as explained in MRI measurements.

Cell Culture and In Vitro Cytotoxicity. NIH-3T3 fibroblasts (American Type Culture Collections, Manassas) were grown as a monolayer in Dulbecco's modified Eagle's medium (DMEM) supplemented with 10% of fetal bovine serum (FBS), 2 mM L-glutamine, 0.25 μg mL^{-1} fungizone, 100 units of penicillin, and 100 μg mL^{-1} streptomycin.

The cell viability was assessed by culturing NIH-3T3 fibroblasts on a 24-well plate at 2.5×10^4 cells per well density. After 24 h, cells were incubated with different Prot-IONP concentrations (1, 2.5, 5, 10, and 20 μM) for 24 h at 37 °C. After 24 h, the cells were washed with PBS and incubated for 4 days under standard cell culture conditions. After this time, cell viability was measured using a resazurin dye (1 mg mL^{-1} in PBS). The cell viability was expressed as the percentage of the ratio between treated and control cells. All experiments were carried out in triplicate.

■ ASSOCIATED CONTENT

Ⓢ Supporting Information

The Supporting Information is available free of charge at https://pubs.acs.org/doi/10.1021/acs.chemmater.2c01746.

Supporting Information contains the protein purity verification, TEM studies, control experiments of the synthetic procedure, CD measurements, relaxometry analysis, XPS measurements, and magnetic characterization (PDF)

■ AUTHOR INFORMATION

Corresponding Authors

Antonio Aires − *Center for Cooperative Research in Biomaterials (CIC biomaGUNE), Basque Research and Technology Alliance (BRTA), Donostia-San Sebastián 20014, Spain;* ⓞ orcid.org/0000-0002-9339-519X; Email: antonio.aires.trapote@gmail.com

Aitziber L. Cortajarena − *Center for Cooperative Research in Biomaterials (CIC biomaGUNE), Basque Research and Technology Alliance (BRTA), Donostia-San Sebastián 20014, Spain; Ikerbasque, Basque Foundation for Science, 48009 Bilbao, Spain;* ⦿ orcid.org/0000-0002-5331-114X; Email: alcortajarena@cicbiomagune.es

Authors

Yilian Fernández-Afonso − *Instituto de Nanociencia y Materiales de Aragón (INMA), CSIC-Universidad de Zaragoza, 50018 Zaragoza, Spain;* ⦿ orcid.org/0000-0002-0970-1917

Gabriela Guedes − *Center for Cooperative Research in Biomaterials (CIC biomaGUNE), Basque Research and Technology Alliance (BRTA), Donostia-San Sebastián 20014, Spain; University of the Basque Country (UPV/EHU), 48940 Leioa, Spain*

Eduardo Guisasola − *Center for Cooperative Research in Biomaterials (CIC biomaGUNE), Basque Research and Technology Alliance (BRTA), Donostia-San Sebastián 20014, Spain;* ⦿ orcid.org/0000-0002-2549-1745

Lucía Gutiérrez − *Instituto de Nanociencia y Materiales de Aragón (INMA), CSIC-Universidad de Zaragoza, 50018 Zaragoza, Spain; Centro de Investigación Biomédica en Red de Bioingeniería, Biomateriales y Nanomedicina (CIBER-BBN), 50018 Zaragoza, Spain;* ⦿ orcid.org/0000-0003-2366-3598

Complete contact information is available at:
https://pubs.acs.org/10.1021/acs.chemmater.2c01746

Notes
The authors declare no competing financial interest.

■ REFERENCES

(1) Reiss, G.; Hütten, A. Applications beyond data storage. *Nat. Mater.* **2005**, *4*, 725−726.

(2) Zhang, H.-w.; Liu, Y.; Sun, S.-h. Synthesis and assembly of magnetic nanoparticles for information and energy storage applications. *Front. Phys. China* **2010**, *5*, 347−356.

(3) Wang, H.; Covarrubias, J.; Prock, H.; Wu, X.; Wang, D.; Bossmann, S. H. Acid-Functionalized Magnetic Nanoparticle as Heterogeneous Catalysts for Biodiesel Synthesis. *J. Phys. Chem. C* **2015**, *119*, 26020−26028.

(4) Tang, S. C. N.; Lo, I. M. C. Magnetic nanoparticles: Essential factors for sustainable environmental applications. *Water Res.* **2013**, *47*, 2613−2632.

(5) Gutierrez, A. M.; Dziubla, T. D.; Hilt, J. Z. Recent advances on iron oxide magnetic nanoparticles as sorbents of organic pollutants in water and wastewater treatment. *Rev. Environ Health Rev* **2017**, *32*, 111−117.

(6) Laurent, S.; Dutz, S.; Häfeli, U. O.; Mahmoudi, M. Magnetic fluid hyperthermia: Focus on superparamagnetic iron oxide nano-particles. *Adv. Colloid Interface Sci.* **2011**, *166*, 8−23.

(7) Zahn, M. Magnetic Fluid and Nanoparticle Applications to Nanotechnology. *J. Nanopart. Res.* **2001**, *3*, 73−78.

(8) Li, X.-B.; Gao, Y.-J.; Wang, Y.; Zhan, F.; Zhang, X.-Y.; Kong, Q.-Y.; Zhao, N.-J.; Guo, Q.; Wu, H.-L.; Li, Z.-J.; Tao, Y.; Zhang, J.-P.; Chen, B.; Tung, C.-H.; Wu, L.-Z. Self-Assembled Framework Enhances Electronic Communication of Ultrasmall-Sized Nano-particles for Exceptional Solar Hydrogen Evolution. *J. Am. Chem. Soc.* **2017**, *139*, 4789−4796.

(9) Wolf, S. A.; Awschalom, D. D.; Buhrman, R. A.; et al. Spintronics: A Spin-Based Electronics Vision for the Future. *Science* **2001**, *294*, 1488−1495.

(10) Cardoso, V. F.; Francesko, A.; Ribeiro, C.; Bañobre-López, M.; Martins, P.; Lanceros-Mendez, S. Advances in Magnetic Nano-particles for Biomedical Applications. *Adv. Health. Mater.* **2018**, *7*, No. 1700845.

(11) Witte, K.; Grüttner, C.; Bodnar, W.; Burkel, E. Magnetic Nanoparticles for Biomedical Applications. In *Encyclopedia of Nanotechnology*; Bhushan, B., Ed.; Springer: Dordrecht, 2016; pp 1842−1850.

(12) Lu, A.-H.; Salabas, E. L.; Schüth, F. Magnetic Nanoparticles: Synthesis, Protection, Functionalization, and Application. *Angew. Chem., Int. Ed.* **2007**, *46*, 1222−1244.

(13) Liu, G.; Gao, J.; Ai, H.; Chen, X. Applications and Potential Toxicity of Magnetic Iron Oxide Nanoparticles. *Small* **2013**, *9*, 1533−1545.

(14) Pankhurst, Q. A.; Connolly, J.; Jones, S. K.; Dobson, J. Applications of magnetic nanoparticles in biomedicine. *J. Phys. D: Appl. Phys.* **2003**, *36*, R167−R181.

(15) Lee, N.; Hyeon, T. Designed synthesis of uniformly sized iron oxide nanoparticles for efficient magnetic resonance imaging contrast agents. *Chem. Soc. Rev.* **2012**, *41*, 2575−2589.

(16) Lee, N.; Yoo, D.; Ling, D.; Cho, M. H.; Hyeon, T.; Cheon, J. Iron Oxide Based Nanoparticles for Multimodal Imaging and Magnetoresponsive Therapy. *Chem. Rev.* **2015**, *115*, 10637−10689.

(17) Du, Y.; Lai, P.; Leung, C.; Pong, P. Design of Super-paramagnetic Nanoparticles for Magnetic Particle Imaging (MPI). *Int. J. Mol. Sci.* **2013**, *14*, 18682−18710.

(18) Ferguson, R. M.; Minard, K. R.; Khandhar, A. P.; Krishnan, K. M. Optimizing magnetite nanoparticles for mass sensitivity in magnetic particle imaging. *Med. Phys.* **2011**, *38*, 1619−1626.

(19) He, J.; Huang, M.; Wang, D.; Zhang, Z.; Li, G. Magnetic separation techniques in sample preparation for biological analysis: A review. *J. Pharm. Biomed. Anal.* **2014**, *101*, 84−101.

(20) Iranmanesh, M.; Hulliger, J. Magnetic separation: its application in mining, waste purification, medicine, biochemistry and chemistry. *Chem. Soc. Rev.* **2017**, *46*, 5925−5934.

(21) Martín, M.; Salazar, P.; Villalonga, R.; Campuzano, S.; Pingarrón, J. M.; González-Mora, J. L. Preparation of core−shell Fe3O4@poly(dopamine) magnetic nanoparticles for biosensor construction. *J. Mater. Chem. B* **2014**, *2*, 739−746.

(22) Liang, Y.-C.; Chang, L.; Qiu, W.; Kolhatkar, A.; Vu, B.; Kourentzi, K.; Lee, T.; Zu, Y.; Willson, R.; Litvinov, D. Ultrasensitive Magnetic Nanoparticle Detector for Biosensor Applications. *Sensors* **2017**, *17*, 1296.

(23) Kossatz, S.; Grandke, J.; Couleaud, P.; Latorre, A.; Aires, A.; Crosbie-Staunton, K.; Ludwig, R.; Dähring, H.; Ettelt, V.; Lazaro-Carrillo, A.; Calero, M.; Sader, M.; Courty, J.; Volkov, Y.; Prina-Mello, A.; Villanueva, A.; Somoza, Á.; Cortajarena, A. L.; Miranda, R.; Hilger, I. Efficient treatment of breast cancer xenografts with multi-

functionalized iron oxide nanoparticles combining magnetic hyperthermia and anti-cancer drug delivery. *Breast Cancer Res.* **2015**, *17*, No. 66.

(24) Blanco-Andujar, C.; Walter, A.; Cotin, G.; Bordeianu, C.; Mertz, D.; Felder-Flesch, D.; Begin-Colin, S. Design of iron oxide-based nanoparticles for MRI and magnetic hyperthermia. *Nanomedicine* **2016**, *11*, 1889−1910.

(25) Wahajuddin; Arora. Superparamagnetic iron oxide nanoparticles: magnetic nanoplatforms as drug carriers. *Int. J. Nanomed.* **2012**, 3445.

(26) Huang, J.; Li, Y.; Orza, A.; Lu, Q.; Guo, P.; Wang, L.; Yang, L.; Mao, H. Magnetic Nanoparticle Facilitated Drug Delivery for Cancer Therapy with Targeted and Image-Guided Approaches. *Adv. Funct. Mater.* **2016**, *26*, 3818−3836.

(27) Kami, D.; Takeda, S.; Itakura, Y.; Gojo, S.; Watanabe, M.; Toyoda, M. Application of Magnetic Nanoparticles to Gene Delivery. *Int. J. Mol. Sci.* **2011**, *12*, 3705−3722.

(28) Jiang, S.; Eltoukhy, A. A.; Love, K. T.; Langer, R.; Anderson, D. G. Lipidoid-Coated Iron Oxide Nanoparticles for Efficient DNA and siRNA delivery. *Nano Lett.* **2013**, *13*, 1059−1064.

(29) Park, J.; An, K.; Hwang, Y.; Park, J.-G.; Noh, H.-J.; Kim, J.-Y.; Park, J.-H.; Hwang, N.-M.; Hyeon, T. Ultra-large-scale syntheses of monodisperse nanocrystals. *Nat. Mater.* **2004**, *3*, 891−895.

(30) Redl, F. X.; Black, C. T.; Papaefthymiou, G. C.; Sandstrom, R. L.; Yin, M.; Zeng, H.; Murray, C. B.; O'Brien, S. P. Magnetic, Electronic, and Structural Characterization of Nonstoichiometric Iron Oxides at the Nanoscale. *J. Am. Chem. Soc.* **2004**, *126*, 14583−14599.

(31) Sun, S.; Zeng, H.; Robinson, D. B.; Raoux, S.; Rice, P. M.; Wang, S. X.; Li, G. Monodisperse MFe_2O_4(M = Fe, Co, Mn) Nanoparticles. *J. Am. Chem. Soc.* **2004**, *126*, 273−279.

(32) Sun, S.; Zeng, H. Size-Controlled Synthesis of Magnetite Nanoparticles. *J. Am. Chem. Soc.* **2002**, *124*, 8204−8205.

(33) Ho, C.-H.; Tsai, C.-P.; Chung, C.-C.; Tsai, C.-Y.; Chen, F.-R.; Lin, H.-J.; Lai, C.-H. Shape-Controlled Growth and Shape-Dependent Cation Site Occupancy of Monodisperse Fe_3O_4 Nanoparticles. *Chem. Mater.* **2011**, *23*, 1753−1760.

(34) Mann, S. *Biomineralization: Principles and Concepts in Bioinorganic Materials Chemistry*; Oxford University Press: New York, 2001, p xii, 198.

(35) De Yoreo, J. J. Principles of Crystal Nucleation and Growth. *Rev. Mineral. Geochem.* **2003**, *54*, 57−93.

(36) Metzler, R. A.; Kim, I. W.; Delak, K.; Evans, J. S.; Zhou, D.; Beniash, E.; Wilt, F.; Abrecht, M.; Chiou, J.-W.; Guo, J.; Coppersmith, S. N.; Gilbert, P. U. P. A. Probing the Organic−Mineral Interface at the Molecular Level in Model Biominerals. *Langmuir* **2008**, *24*, 2680−2687.

(37) Xie, J.; Ping, H.; Tan, T.; Lei, L.; Xie, H.; Yang, X.-Y.; Fu, Z. Bioprocess-inspired fabrication of materials with new structures and functions. *Prog. Mater. Sci.* **2019**, *105*, No. 100571.

(38) Blakemore, R. Magnetotactic bacteria. *Science* **1975**, *190*, 377−379.

(39) Bellini, S. On a unique behavior of freshwater bacteria. *Chin. J. Oceanol. Limnol.* **2009**, *27*, 3−5.

(40) Gorby, Y. A.; Beveridge, T. J.; Blakemore, R. P. Characterization of the bacterial magnetosome membrane. *J. Bacteriol.* **1988**, *170*, 834−841.

(41) Grunberg, K.; Muller, E. C.; Otto, A.; Reszka, R.; Linder, D.; Kube, M.; Reinhardt, R.; Schuler, D. Biochemical and Proteomic Analysis of the Magnetosome Membrane in Magnetospirillum gryphiswaldense. *Appl. Environ. Microbiol.* **2004**, *70*, 1040−1050.

(42) Arakaki, A.; Webb, J.; Matsunaga, T. A Novel Protein Tightly Bound to Bacterial Magnetic Particles inMagnetospirillum magneticumStrain AMB-1. *J. Biol. Chem.* **2003**, *278*, 8745−8750.

(43) Galloway, J. M.; Arakaki, A.; Masuda, F.; Tanaka, T.; Matsunaga, T.; Staniland, S. S. Magnetic bacterial protein Mms6 controls morphology, crystallinity and magnetism of cobalt-doped magnetite nanoparticles in vitro. *J. Mater. Chem.* **2011**, *21*, 15244.

(44) Amemiya, Y.; Arakaki, A.; Staniland, S. S.; Tanaka, T.; Matsunaga, T. Controlled formation of magnetite crystal by partial oxidation of ferrous hydroxide in the presence of recombinant magnetotactic bacterial protein Mms6. *Biomaterials* **2007**, *28*, 5381−5389.

(45) Wang, L.; Prozorov, T.; Palo, P. E.; Liu, X.; Vaknin, D.; Prozorov, R.; Mallapragada, S.; Nilsen-Hamilton, M. Self-Assembly and Biphasic Iron-Binding Characteristics of Mms6, A Bacterial Protein That Promotes the Formation of Superparamagnetic Magnetite Nanoparticles of Uniform Size and Shape. *Biomacromolecules* **2012**, *13*, 98−105.

(46) Prozorov, T.; Mallapragada, S. K.; Narasimhan, B.; Wang, L.; Palo, P.; Nilsen-Hamilton, M.; Williams, T. J.; Bazylinski, D. A.; Prozorov, R.; Canfield, P. C. Protein-Mediated Synthesis of Uniform Superparamagnetic Magnetite Nanocrystals. *Adv. Funct. Mater.* **2007**, *17*, 951−957.

(47) Aires, A.; Sousaraei, A.; Möller, M.; Cabanillas-Gonzalez, J.; Cortajarena, A. L. Boosting the Photoluminescent Properties of Protein-Stabilized Gold Nanoclusters through Protein Engineering. *Nano Lett.* **2021**, *21*, 9347−9353.

(48) Aires, A.; Llarena, I.; Moller, M.; Castro-Smirnov, J.; Cabanillas-Gonzalez, J.; Cortajarena, A. L. A Simple Approach to Design Proteins for the Sustainable Synthesis of Metal Nanoclusters. *Angew. Chem., Int. Ed.* **2019**, *58*, 6214−6219.

(49) Aires, A.; Fernández-Luna, V.; Fernández-Cestau, J.; Costa, R. D.; Cortajarena, A. L. White-emitting Protein-Metal Nanocluster Phosphors for Highly Performing Biohybrid Light-Emitting Diodes. *Nano Lett.* **2020**, *20*, 2710−2716.

(50) Aires, A.; Möller, M.; Cortajarena, A. L. Protein Design for the Synthesis and Stabilization of Highly Fluorescent Quantum Dots. *Chem. Mater.* **2020**, *32*, 5729−5738.

(51) Lopez-Martinez, E.; Gianolio, D.; Garcia-Orrit, S.; Vega-Mayoral, V.; Cabanillas-Gonzalez, J.; Sanchez-Cano, C.; Cortajarena, A. L. Tuning the Optical Properties of Au Nanoclusters by Designed Proteins. *Adv. Opt. Mater.* **2021**, *10*, No. 2101332.

(52) Dheyab, M. A.; Aziz, A. A.; Jameel, M. S.; Noqta, O. A.; Khaniabadi, P. M.; Mehrdel, B. Simple rapid stabilization method through citric acid modification for magnetite nanoparticles. *Sci. Rep.* **2020**, *10*, No. 10793.

(53) Rawlings, A. E.; Bramble, J. P.; Hounslow, A. M.; Williamson, M. P.; Monnington, A. E.; Cooke, D. J.; Staniland, S. S. Ferrous Iron Binding Key to Mms6 Magnetite Biomineralisation: A Mechanistic Study to Understand Magnetite Formation Using pH Titration and NMR Spectroscopy. *Chem. − Eur. J.* **2016**, *22*, 7885−7894.

(54) Main, E. R.; Xiong, Y.; Cocco, M. J.; D'Andrea, L.; Regan, L. Design of stable alpha-helical arrays from an idealized TPR motif. *Structure* **2003**, *11*, 497−508.

(55) Magliery, T. J.; Regan, L. Beyond Consensus: Statistical Free Energies Reveal Hidden Interactions in the Design of a TPR Motif. *J. Mol. Biol.* **2004**, *343*, 731−745.

(56) Feng, S.; Wang, L.; Palo, P.; Liu, X.; Mallapragada, S.; Nilsen-Hamilton, M. Integrated Self-Assembly of the Mms6 Magnetosome Protein to Form an Iron-Responsive Structure. *Int. J. Mol. Sci.* **2013**, *14*, 14594−14606.

(57) Aires, A.; Maestro, D.; Ruiz del Rio, J.; Palanca, A. R.; Lopez-Martinez, E.; Llarena, I.; Geraki, K.; Sanchez-Cano, C.; Villar, A. V.; Cortajarena, A. L. Engineering multifunctional metal/protein hybrid nanomaterials as tools for therapeutic intervention and high-sensitivity detection. *Chem. Sci.* **2021**, *12*, 2480−2487.

(58) Uribe, K. B.; Guisasola, E.; Aires, A.; López-Martínez, E.; Guedes, G.; Sasselli, I. R.; Cortajarena, A. L. Engineered Repeat Protein Hybrids: The New Horizon for Biologic Medicines and Diagnostic Tools. *Acc. Chem. Res.* **2021**, *54*, 4166−4177.

(59) Rohrer, M.; Bauer, H.; Mintorovitch, J.; Requardt, M.; Weinmann, H.-J. Comparison of Magnetic Properties of MRI Contrast Media Solutions at Different Magnetic Field Strengths. *Invest. Radiol.* **2005**, *40*, 715−724.

(60) Wahsner, J.; Gale, E. M.; Rodríguez-Rodríguez, A.; Caravan, P. Chemistry of MRI Contrast Agents: Current Challenges and New Frontiers. *Chem. Rev.* **2019**, *119*, 957−1057.

(61) Jeon, M.; Halbert, M. V.; Stephen, Z. R.; Zhang, M. Iron Oxide Nanoparticles as T1 Contrast Agents for Magnetic Resonance Imaging: Fundamentals, Challenges, Applications, and Prospectives. *Adv. Mater.* **2020**, *33*, No. 1906539.

(62) Close, D. M.; Wardman, P. Calculation of Standard Reduction Potentials of Amino Acid Radicals and the Effects of Water and Incorporation into Peptides. *J. Phys. Chem. A* **2018**, *122*, 439−445.

(63) Moulder, J. F.; Stickle, W. F.; Sobol, W. M.; Bomben, K. D.; Chastain, J. *Handbook of X-Ray Photoelectron Spectroscopy*; Chastain, J., Ed.; Perkin-Elmer Corporation: Minnesota, 1992.

(64) Descostes, M.; Mercier, F.; Thromat, N.; Beaucaire, C.; Gautier-Soyer, M. Use of XPS in the determination of chemical environment and oxidation state of iron and sulfur samples: constitution of a data basis in binding energies for Fe and S reference compounds and applications to the evidence of surface species of an oxidized pyrite in a carbonate medium. *Appl. Surf. Sci.* **2000**, *165*, 288−302.

(65) Zhou, Z.; Yang, L.; Gao, J.; Chen, X. Structure-Relaxivity Relationships of Magnetic Nanoparticles for Magnetic Resonance Imaging. *Adv. Mater.* **2019**, *31*, No. 1804567.

(66) Pellico, J.; Ruiz-Cabello, J.; Fernández-Barahona, I.; Gutiérrez, L.; Lechuga-Vieco, A. V.; Enríquez, J. A.; Morales, M. P.; Herranz, F. One-Step Fast Synthesis of Nanoparticles for MRI: Coating Chemistry as the Key Variable Determining Positive or Negative Contrast. *Langmuir* **2017**, *33*, 10239−10247.

(67) Zhao, Z.; Li, M.; Zeng, J.; Huo, L.; Liu, K.; Wei, R.; Ni, K.; Gao, J. Recent advances in engineering iron oxide nanoparticles for effective magnetic resonance imaging. *Bioact. Mater.* **2022**, *12*, 214−245.

(68) Osborne, E. A.; Jarrett, B. R.; Tu, C.; Louie, A. Y. Modulation of T2 Relaxation Time by Light-Induced, Reversible Aggregation of Magnetic Nanoparticles. *J. Am. Chem. Soc.* **2010**, *132*, 5934−5935.

(69) Brown, K. A.; Vassiliou, C. C.; Issadore, D.; Berezovsky, J.; Cima, M. J.; Westervelt, R. M. Scaling of transverse nuclear magnetic relaxation due to magnetic nanoparticle aggregation. *J. Magn. Magn. Mater.* **2010**, *322*, 3122−3126.

(70) Kajander, T.; Cortajarena, A. L.; Regan, L. Consensus Design as a Tool for Engineering Repeat Proteins. In *Protein Design, MIMB: Methods in Molecular Biology*; Guerois, R.; de la Paz, M. L., Eds.; Humana Press, 2006; Vol. *340*, pp 151−170.

(71) Cortajarena, A. L.; Mochrie, S. G.; Regan, L. Modulating repeat protein stability: The effect of individual helix stability on the collective behavior of the ensemble. *Protein Sci.* **2011**, *20*, 1042−1047.

(72) Yamashita, T.; Hayes, P. Analysis of XPS spectra of Fe2+ and Fe3+ ions in oxide materials. *Appl. Surf. Sci.* **2008**, *254*, 2441−2449.